NASA / TM—1998-207422 AIAA–98–2294

Supersonic Coaxial Jets: Noise Predictions and Measurements

Milo D. Dahl
Lewis Research Center, Cleveland, Ohio

Dimitri Papamoschou
University of California, Irvine, California

Ray Hixon
Lewis Research Center, Cleveland, Ohio

May 1998

The NASA STI Program Office . . . in Profile

Since its founding, NASA has been dedicated to the advancement of aeronautics and space science. The NASA Scientific and Technical Information (STI) Program Office plays a key part in helping NASA maintain this important role.

The NASA STI Program Office is operated by Langley Research Center, the Lead Center for NASA's scientific and technical information. The NASA STI Program Office provides access to the NASA STI Database, the largest collection of aeronautical and space science STI in the world. The Program Office is also NASA's institutional mechanism for disseminating the results of its research and development activities. These results are published by NASA in the NASA STI Report Series, which includes the following report types:

- TECHNICAL PUBLICATION. Reports of completed research or a major significant phase of research that present the results of NASA programs and include extensive data or theoretical analysis. Includes compilations of significant scientific and technical data and information deemed to be of continuing reference value. NASA's counterpart of peer-reviewed formal professional papers but has less stringent limitations on manuscript length and extent of graphic presentations.

- TECHNICAL MEMORANDUM. Scientific and technical findings that are preliminary or of specialized interest, e.g., quick release reports, working papers, and bibliographies that contain minimal annotation. Does not contain extensive analysis.

- CONTRACTOR REPORT. Scientific and technical findings by NASA-sponsored contractors and grantees.

- CONFERENCE PUBLICATION. Collected papers from scientific and technical conferences, symposia, seminars, or other meetings sponsored or cosponsored by NASA.

- SPECIAL PUBLICATION. Scientific, technical, or historical information from NASA programs, projects, and missions, often concerned with subjects having substantial public interest.

- TECHNICAL TRANSLATION. English-language translations of foreign scientific and technical material pertinent to NASA's mission.

Specialized services that complement the STI Program Office's diverse offerings include creating custom thesauri, building customized data bases, organizing and publishing research results . . . even providing videos.

For more information about the NASA STI Program Office, see the following:

- Access the NASA STI Program Home Page at ***http://www.sti.nasa.gov***

- E-mail your question via the Internet to help@sti.nasa.gov

- Fax your question to the NASA Access Help Desk at (301) 621-0134

- Telephone the NASA Access Help Desk at (301) 621-0390

- Write to:
  NASA Access Help Desk
  NASA Center for AeroSpace Information
  7121 Standard Drive
  Hanover, MD 21076

NASA / TM—1998-207422 AIAA–98–2294

Supersonic Coaxial Jets: Noise Predictions and Measurements

Milo D. Dahl
Lewis Research Center, Cleveland, Ohio

Dimitri Papamoschou
University of California, Irvine, California

Ray Hixon
Lewis Research Center, Cleveland, Ohio

Prepared for the
Fourth Aeroacoustics Conference
cosponsored by the American Institute of Aeronautics and Astronautics and
the Confederation of European Aerospace Societies
Toulouse, France, June 2–4, 1998

National Aeronautics and
Space Administration

Lewis Research Center

May 1998

Available from

NASA Center for Aerospace Information
7121 Standard Drive
Hanover, MD 21076
Price Code: A03

National Technical Information Service
5287 Port Royal Road
Springfield, VA 22100
Price Code: A03

SUPERSONIC COAXIAL JETS: NOISE PREDICTIONS AND MEASUREMENTS

Milo D. Dahl*
NASA Lewis Research Center
Cleveland, OH 44135

Dimitri Papamoschou‡
University of California, Irvine
Irvine, CA 92697

Ray Hixon†
Institute for Computational Mechanics in Propulsion
NASA Lewis Research Center
Cleveland, OH 44135

ABSTRACT

The noise from perfectly expanded coaxial jets was measured in an anechoic chamber for different operating conditions with the same total thrust, mass flow, and exit area. The shape of the measured noise spectrum at different angles to the jet axis was found to agree with spectral shapes for single, axisymmetric jets. Based on these spectra, the sound was characterized as being generated by large-scale turbulent structures or fine-scale turbulence. Modeling the large-scale structures as instability waves, a stability analysis was conducted for the coaxial jets to identify the growing and decaying instability waves in each shear layer and predict their noise radiation pattern outside the jet. When compared to measured directivity, the analysis identified the region downstream of the outer potential core, where the two shear layers were merging, as the source of the peak radiated noise where instability waves, with their origin in the inner shear layer, reach their maximum amplitude. Numerical computations were also performed using a linearized Euler equation solver. Those results were compared to both the results from the instability wave analysis and to measured data.

INTRODUCTION

Supersonic jet noise is generated by mechanisms associated with fine-scale turbulence, large-scale turbulent structures and shocks. Depending on the jet operating conditions and the structure of the exhausting flow field, each of these noise generating mechanisms can contribute to the noise radiated to the far field at a given frequency and in differing amounts as a function of the direction from the jet to the observer. Since jet noise continues to be of concern in the development of advanced aircraft, it is hoped that a greater understanding of the jet noise generation process will lead to means by which the noise may be reduced while maintaining acceptable propulsion system performance.

One concept for reducing supersonic jet noise is to replace the single stream jet with a dual stream, coaxial jet. Recent separate studies have considered this concept analytically,[1] numerically,[2] and experimentally.[3] The initial conditions used in these studies set the jet for shock-free, perfectly expanded flow. The resulting noise is generated by turbulent mechanisms that primarily radiate noise toward the downstream arc of the jet. If the jet speed is sufficiently supersonic, the large-scale turbulent structures become dominant noise radiators when their phase velocity is supersonic relative to the speed of sound in the adjacent lower speed or ambient flow. The addition of a lower speed secondary flow to a single supersonic jet modifies the growth rate and phase velocity of the large structures in the primary flow shear layer and, if the jet conditions are properly chosen, it has been shown experimentally that applying the secondary flow can lead to lower levels of radiated noise.[4] It is the purpose of this paper to compare and discuss the results from two methods of calculating the radiated supersonic jet noise and the results from experimental measurements.

For noise generated by large-scale structures, the analysis uses the instability wave noise generation model. The large-scale structures that exist in the growing jet shear layer are modeled as instability waves that initially grow rapidly and then decay in the axial direction as the shear layer widens. Tam and Burton[5] developed a matched asymptotic solution for the noise radiated from the the instability waves in the slowly growing shear layer of a single stream, supersonic, axisymmetric jet. The equations

*Research Scientist, member AIAA
†Senior Research Associate, member AIAA
‡Associate Professor, member AIAA

developed were used to calculate the stability characteristics and the radiated noise directivity of an instability wave at a single frequency and a single mode number. Their results showed good comparisons with measurements from low Reynolds number jet experiments. Comparisons of calculated results with measured data were also made with high-speed jets[6] and high temperature jets.[7] This single mode method was later extended to include the addition of multiple modes using stochastic theory.[8]

The instability wave noise generation model was applied to supersonic coaxial jets by Dahl and Morris.[1] The ability to complete the stability and noise calculations depended on computing numerically the mean flow for both velocity and density fields.[9] Thus, a variety of jet operating conditions could be modeled, including both normal and inverted velocity profiles, and the stability and noise generation could be studied due to velocity and density ratio changes between the two jet streams and area ratio changes at the nozzle exit. The results were focussed on the Kelvin-Helmholtz type inflectional instabilities. Other modes can exist in supersonic jets that may or may not radiate noise.[10] Using the eigenvalue problem approach of the instability wave model, each of these modes would have to be found and investigated separately to determine any ability for them to radiate noise. Direct numerical calculations allow all radiating modes to develop naturally.

Hixon et al.[2] applied a numerical approach for the linearized Euler equations to compute the near field noise radiated from supersonic coaxial jets. Within the limitations inherent in using linearized equations, the method fully accounts for the non-parallel flow effects and the presence of multiple frequencies. In principle, the method simultaneously describes both the near and far sound field; however, it requires a known mean flow field.[9] Based on computed noise radiation patterns for coaxial jets where both flow streams had supersonic Mach numbers, the linearized Euler results showed that noise radiation occurred from the presence of both Kelvin-Helmholtz type and supersonic type instabilities.

Recently, Papamoschou[3] began small scale experiments using perfectly expanded coaxial jets. The purpose was to explore flow conditions where Mach wave radiation is reduced from that of a single jet when a secondary stream is applied at proper conditions. Mach wave radiation is the source of the dominant noise generated by instability waves convecting supersonically in the shear layer of a jet. They can be generated by both the Kelvin-Helmholtz type and the supersonic type instability modes. According to the model presented by Papamoschou, if the relative phase velocities of the Mach wave generating disturbances can be made subsonic in both shear layers, then Mach wave radiation can be reduced. The success of this approach has been shown in flow visualizations[3] and in acoustic field measurements.[4] The experimental facilities that have been built allow acoustic data to be taken for noise generated by perfectly expanded coaxial jets, the conditions on which the instability wave and the linearized Euler analyzes are based. Thus, the opportunity exists to compare the calculated results to measured data where Mach wave radiation exists.

NUMERICAL CALCULATIONS

The calculation of the noise radiated from a supersonic jet was based on two different approaches. In the first, the linear, inviscid, instability wave theory was applied. A thin free shear layer containing an inflection point in the mean velocity profile is inherently unstable. Initially, an instability wave in the shear layer grows rapidly. This wave growth rate decreases as the shear layer grows until eventually, the shear layer is too thick to support unstable waves and the wave amplitude decreases until it disappears. The growth and decay of the instability wave produces a range of wave number components. Those components that have a phase velocity that is supersonic relative to the ambient conditions will radiate noise to the far field.

The second approach involves the numerical solution of the linearized Euler equations. This method also neglects the viscous effects in computing the large-scale dynamics in a free shear flow. The problem of matching the disturbance generated by an unstable shear layer to the acoustic field outside the jet does not arise since both are calculated simultaneously. Outlines of both computational approaches are given next.

Instability Waves

The shear layer of a supersonic jet grows slowly in the axial direction. This slow change in the axial direction compared to more rapid changes in the radial direction allows a locally parallel flow approximation to be used in solving for the disturbance quantities. All the fluctuating disturbance quantities are represented as waves traveling through a nonuniform medium. For example, the pressure disturbances are given by

$$p'(r,\theta,x,t) = p(r,x) \times \exp\left[i\left(\int_0^x \alpha(\chi)\,d\chi + n\theta - \omega t\right)\right] \quad (1)$$

where $p(r,x)$ represents the radial (r) distribution of the pressure disturbance at each axial (x) location, $\alpha(x)$ is the local complex wave number ($\alpha = \alpha_r + i\alpha_i$ and $-\alpha_i$ is the local growth rate), θ is the azimuthal angle, n is the mode number, and $\exp(-i\omega t)$ is the harmonic time dependence. The linearized equations governing the disturbances can be combined

to obtain a single equation,

$$\frac{\partial^2 p}{\partial r^2} + \left[\frac{1}{r} + \frac{2\alpha}{\omega - \alpha\overline{u}}\frac{\partial \overline{u}}{\partial r} - \frac{1}{\overline{\rho}}\frac{\partial \overline{\rho}}{\partial r}\right]\frac{\partial p}{\partial r} + \left[\overline{\rho}M_j^2(\omega - \alpha\overline{u})^2 - \frac{n^2}{r^2} - \alpha^2\right]p = 0\,. \quad (2)$$

This equation has been nondimensionalized by the exit conditions of the primary jet: spatial coordinates by R_1, velocity by U_1, and density by ρ_1. The time and radial frequency are made dimensionless by U_1/R_1 and the pressure by $\rho_1 U_1^2$. To solve equation (2) at each axial location, the radial and axial variation of the mean flow velocity $\overline{u}$ and density $\overline{\rho}$ must be known quantities.

The general solution to equation (2) can be written as the sum of two general linearly independent solutions that are functions of the radial and axial coordinates. Outside the jet, the mean flow becomes uniform and equation (2) takes the form of Bessel's equation. This equation is used to enforce the boundary condition that the disturbances generated in the shear layer must decay away from the shear layer, that is

$$p \sim H_n^{(1)}(i\lambda(\alpha)r) \quad (3)$$

where

$$\lambda(\alpha) = \left[\alpha^2 - \overline{\rho}_\infty M_j^2(\omega - \alpha\overline{u}_\infty)^2\right]^{1/2}. \quad (4)$$

and $H_n^{(1)}$ is the nth-order Hankel function of the first kind. At the jet axis, $\partial p/\partial r$ is set to zero for $n = 0$, and $p = 0$ for $n > 0$.

Outside the jet, the governing equations control acoustic disturbances with the same length scales in all directions. The solution to these outer equations is found by Fourier transforming the disturbance variables from the physical axial coordinate x to the wave number coordinate η. The matched asymptotic expansion technique is applied to construct a formula for the pressure disturbances outside the jet generated by the instability wave in the shear layer,

$$p(r,\theta,x,t) = \int_{-\infty}^{\infty} g(\eta)H_n^{(1)}(i\lambda(\eta)r)e^{i\eta x}e^{in\theta}e^{-i\omega t}d\eta \quad (5)$$

where

$$g(\eta) = \frac{1}{2\pi}\int_{-\infty}^{\infty} A_0 \exp\left[i\int_0^x \alpha(\chi)\,d\chi\right]e^{-i\eta x}dx. \quad (6)$$

Equation (6) describes the Fourier transform into wave number space of the axial evolution of the nth mode spatial instability wave at a fixed real frequency ω with unknown initial amplitude A_0. This equation describes the source in a noise radiation problem. Then, equation (5) multiplies this source term, $g(\eta)$, by a Hankel function to propagate the generated wave outside the jet and inverts the Fourier transform back to physical space.

Equation (2) and its boundary conditions create an eigenvalue problem for α that is solved using a finite difference approximation. The local eigenvalue is found from the resulting diagonal matrix using a Newton-Raphson iteration technique for refinement yielding the local growth rate, $-\alpha_i$, and phase velocity, $c_{ph} = \omega/\alpha_r$. Once α is determined at each axial location, the wave number spectrum is calculated by equation (6) followed by the acoustic pressure from equation (5). The details are given in Dahl and Morris.[1]

Linearized Euler

The Euler equations are linearized about a known mean flow using a disturbance with a periodic distribution in the azimuthal direction. For example, the pressure disturbance for a particular mode n is given by

$$p'_n = \varepsilon A(r,x)e^{i(\omega+\phi)t} \quad (7)$$

where ε is a small initial amplitude (set to 0.001), $A(r,x)$ is a spatial distribution, and ϕ is a random phase. Separating the equations by azimuthal modes, the linearized Euler equations are written in cylindrical coordinates as

$$\frac{\partial}{\partial t}(r\overline{Q}) + \frac{\partial}{\partial x}(r\overline{F}) + \frac{\partial}{\partial r}(r\overline{G}) = \overline{S} - in\overline{H} \quad (8)$$

where $\overline{Q}$, $\overline{F}$, $\overline{G}$, $\overline{S}$, and $\overline{H}$ are given in Hixon et al.[2] Equation (8) is also nondimensionalized by the primary jet exit conditions in the same manner as used in equation (2). The numerical scheme is a high-accuracy MacCormack-type scheme developed by Hixon,[11] which has been previously tested in linearized Euler equation solutions of coaxial supersonic jet noise.[2]

EXPERIMENTAL METHOD

Experiments were conducted in a coaxial jet facility with capability of supplying mixtures of helium and air to the inner and outer flows, depicted in Figure 1. The inner nozzles, of 12.7-mm exit diameter, were designed by the method of characteristics for Mach numbers 1.5, 1.75, and 2.0. The outer nozzle formed a smooth contraction terminating in an exit diameter of 21.6 mm. Both flows exhausted into ambient, still air. Details of the facility can be found in Ref. [3].

Helium-air mixtures allow variation of the gas constant R and thus of the velocity at fixed Mach number and fixed total temperature. A jet composed of helium-oxygen mixture simulates very accurately the speed of sound, velocity, and growth rate of a hot jet at the same density ratio.[3] In this experiment, the mixtures were accurately metered so that

the uncertainty in the gas constant was less than 5%. For all cases, the total temperature of the gas mixture was around 300° K. The exit density can be translated to the temperature of the simulated hot jet via the relation $T/T_\infty = \rho_\infty/\rho$. The experimental Mach numbers, velocity ratios, and simulated temperature ratios are the same as those used in the numerical calculations, shown in Table 1. Typical Reynolds numbers in the experiments were 5×10^5 for the inner flow, based on jet diameter, and 5×10^4 for the outer flow, based on annulus thickness.

The jet noise was recorded by a one-eighth inch condenser microphone connected to a preamplifier and power supply (Bruel & Kjaer Models 4138, 2670, and 5935L, respectively). The microphone has a frequency response up to 150 kHz and was sampled at 400 kHz by a fast analog-to-digital board (National Instruments AT-MIO-16E1) installed in a Pentium Pro computer. Each recording consisted of 54280 samples (135 ms), corresponding to passage of about 10,000 eddies the size of the inner-jet diameter. The signal was high-pass filtered at 500 Hz by a Butterworth filter to remove spurious low-frequency noise. The power spectrum of each recording was computed using a 1024-point FFT with a full Hanning window. The microphone was calibrated daily before each series of recordings (Bruel & Kjaer Model 4231 calibrator).

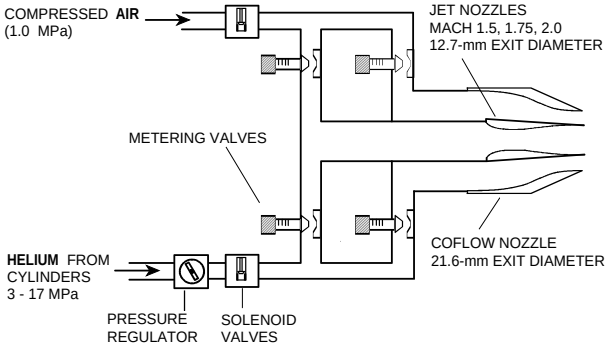

Figure 1: Schematic of the supersonic coaxial jet facility.

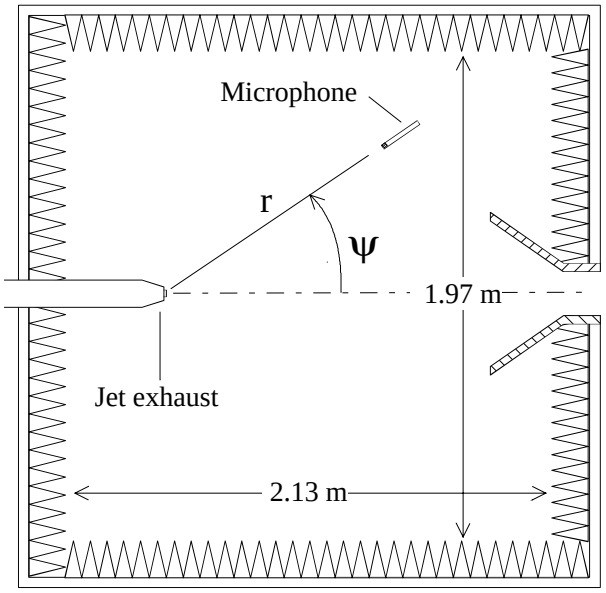

Figure 2: Anechoic chamber and positioning of jet and microphone.

Sound measurements were conducted inside an anechoic chamber, approximately 8-m^3 in internal size, lined with acoustic wedges (Sonex) with an absorption coefficient higher than 0.99 for frequencies above 400 Hz. The microphone was mounted on an arm which pivoted around an axis passing through the center of the jet exit. This arrangement enabled sound measurement at a variety of radial (r) and polar (ψ) positions. The setup is shown in Figure 2. For each measurement, the power spectrum was computed according to

$$S(f) \;=\; S_{\rm raw}(f) + \Delta S_{\rm fr}(f) + \Delta S_{\rm ff}(f,\phi) \qquad (9)$$

where $S_{\rm raw}(f)$ is the raw spectrum of $p'/p_{\rm ref}$ ($p_{\rm ref} = 20\ \mu$Pa), $\Delta S_{\rm fr}(f)$ is the frequency-response correction, $\Delta S_{\rm ff}(f,\phi)$ is the free-field correction, and ϕ is the angle between the sound propagation vector and the microphone axis which for the present experiments was 0 deg. The sound pressure level (SPL) spectrum is given by

$$\mathrm{SPL}(f) \;=\; 10\ \log_{10} S(f) \qquad (10)$$

and the overall sound pressure level (OASPL), which describes the contribution of all measured frequencies, is computed from the integral

$$\mathrm{OASPL} \;=\; 10\ \log_{10} \int_0^\infty S(f) df. \qquad (11)$$

RESULTS

Three flow condition cases for which calculations were conducted and experimental data were collected are shown in Table 1. The three cases were chosen such that they all have the same mass flow, thrust, and exit area. These type of conditions were recommended by Tanna[12] for comparing noise results of different coaxial jets. For supersonic coaxial jets with a higher speed primary stream surrounded by a lower speed secondary stream, the condition of perfect expansion set the primary stream Mach number to the design Mach number of the nozzle. The remaining operating conditions for these cases, referred to as the constant flow condition cases, were found by iteration until all cases had the same mass flow and thrust for the given coaxial nozzle exit area.

Case	M_1	T_1/T_∞	M_2	T_2/T_∞	U_2/U_1
1	1.50	3.03	1.09	1.89	0.58
2	1.75	2.64	0.88	1.65	0.40
3	2.00	1.89	0.52	1.18	0.22

(Constant Thrust and Constant Mass Flow)
$T_\infty = 300\,K$

Table 1: Operating conditions for supersonic coaxial jet calculations.

Case	$\overline{\gamma}$	$\overline{R}$	$\overline{T}_1/T_\infty$	$\overline{T}_2/T_\infty$	M_{c1}	M_{c2}
1	1.56	285.3	3.04	1.89	0.45	1.08
2	1.54	292.9	2.65	1.65	0.97	0.78
3	1.48	304.3	1.81	1.23	1.56	0.29

$\overline{R}$ in $m^2/s^2\,{}^\circ K$

Table 2: Averaged gas properties and convective Mach numbers for supersonic coaxial jet calculations.

An additional criterion was to hold the temperature ratio constant between the two jet streams. For these cases, $T_2/T_1 = 0.62$. Hence, the primary variable parameter for the constant flow condition cases is the velocity ratio between the streams.

In performing the stability and noise calculations for both numerical methods, the mean flow for the coaxial jet was provided from the method of Dahl and Morris.[9] The experiments used a mixture of gases to simulate the effects of temperature by changing the gas mixture density. Each stream then had its own gas constant and ratio of specific heats. The mean flow code, however, was designed for a single type of gas with varying temperature. Thus, to complete the mean flow calculations, both an average gas constant and an average specific heat ratio were used with the result that temperature ratios were slightly different than those used in the experiments as indicated in Table 2.

Measured Spectra

Spectra measured at $r/D_1 = 80$ are shown in Figure 3 for the three constant flow condition cases at four angles from the exit axis, ψ in Figure 2. (Note that in the context of large distances from the jet, the spherical radius shown in Figure 2 is used. Otherwise, the radius r is the cylindrical coordinate measured from the jet exit axis.) The data are plotted in terms of a Strouhal number $St = fD_1/U_1$ over the range 0 to 0.5. The spectra have similar shape for all three conditions. At low angles, there is a well defined peak at lower Strouhal numbers. The 20 degree spectra peak at about $St = 0.04$ and the 40 degree spectra peak at about $St = 0.06$. As the angle increases, the peak becomes broader and moves to higher Strouhal number so that at 60 degrees, the peak is at about $St = 0.14$. Finally, at 80 degrees, the spectra have broadened out until there is no clear peak shown for the data when plotted on this scale.

The spectral behavior, shown in Figure 3, was previously found in data taken on subsonic coaxial jets[13] and on supersonic coaxial jets that contained shocks.[14] Single, $M = 2$, perfectly expanded supersonic jets also showed this behavior.[15] Stone et al.[16] developed an empirical model for coaxial jet noise prediction using the experimental observation that spectra have a similar shape between single and coaxial jets with a normal velocity profile. The peaks of the coaxial jet spectra were shifted in frequency and direction due to the velocity and temperature ratio changes between the two streams. Recently, Tam et al.[17] correlated the spectral measurements from a large number of single stream jets to derive a pair of similarity spectra that characterized the two types of turbulent mixing noise. One spectrum had a broad peak and characterized the noise from fine-scale mixing. The other spectrum had a narrower, well defined peak. It characterized the noise from large-scale mixing. Based on compressibility arguments, they stated that both noise generating mechanisms could exist to some degree in both sub-

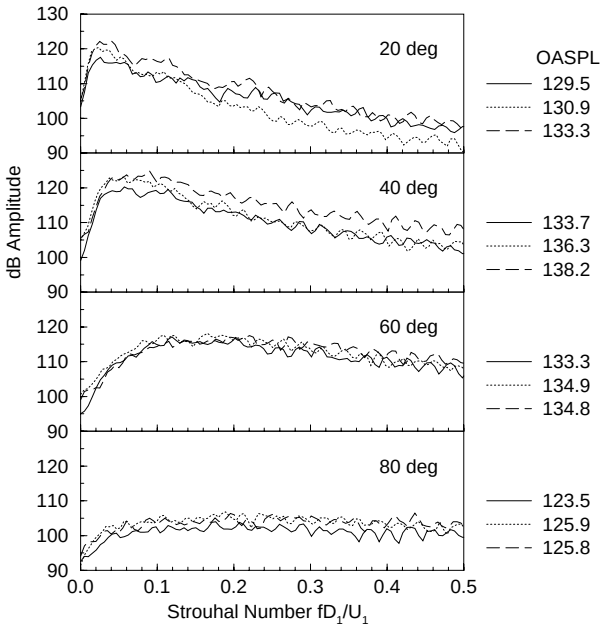

Figure 3: Sound pressure level spectra measured at $r/D_1 = 80$ and at four angles from the downstream jet axis. Three constant flow conditions: (————) Case 1; (· · · · · ·) Case 2; (— — —) Case 3.

sonic and supersonic jets. Their spectra agreed well with data from axisymmetric, rectangular, and elliptic single stream jets. Considering the spectral similarity used by Stone et al.[16] for both single and coaxial jets, there is no reason why Tam's spectra should not apply as well to coaxial jets. A comparison between the jet noise similarity spectra and the measured spectra for Case 1 is shown in Figure 4. The frequency of the spectrum has been normalized by the peak frequency and plotted on a logarithmic scale. In the figure, the similarity spectra are adjusted in amplitude to match the spectra to the measured data. At 20, 40, and 60 degrees, the measured spectra are plotted with the large-scale turbulent mixing noise similarity spectrum. This jet has a supersonic primary stream surrounded by a sonic secondary stream and these results indicate that, in the downstream direction from the jet, noise due to large structures dominates. At 80 degrees, the measured spectrum is no longer characterized by the large-scale similarity spectrum, but is well characterized by the fine-scale turbulent mixing similarity spectrum. This agrees with data comparisons using single stream supersonic jets. Given the similar spectral shapes for the three cases shown in Figure 3, the similarity spectra were also found to apply as well to Cases 2 and 3 with subsonic secondary streams surrounding a supersonic primary stream. Next, we will identify the source region for the dominant noise radiation.

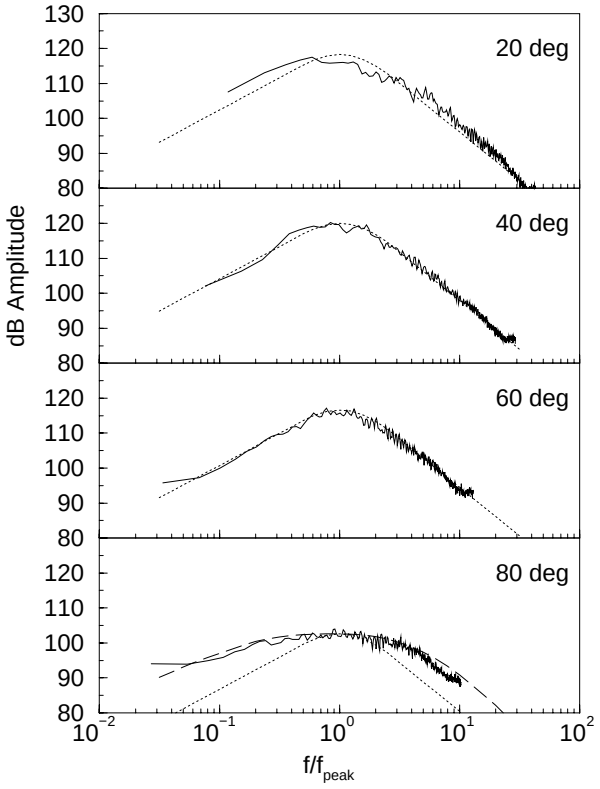

Figure 4: Sound pressure level spectra measured at $r/D_1 = 80$ for Case 1 compared to jet noise similarity spectra given in Ref. [17]. (————) measured data; (· · · · · ·) large-scale turbulent structure noise similarity spectrum; (— — —) fine-scale turbulence noise similarity spectrum.

Stability Analysis

The results from the stability calculations for Case 1 are shown in Figure 5 for the outer shear layer and in Figure 6 for the inner shear layer. Each figure shows an illustration of the mean velocity field by outlining the edges of the two potential cores and identifies the region over which the two shear layers merge into a single shear layer. The remaining parts of the figure show the local phase velocity, c_{ph}, the local growth rate, $-\alpha_i$, and the instability wave amplitude when the initial amplitude is set to one. The results shown here are for the $n = 1$ mode since this mode typically had the largest wave amplitude.

For the outer shear layer, Figure 5 shows that the instability wave grows and decays slowly at low Strouhal numbers. The outer shear layer has a larger velocity difference than the inner shear layer and sustains the growth of these longer wavelength instability waves further downstream to where the shear layers have merged. At higher Strouhal numbers, the instability wave grows more rapidly and decays more significantly before the outer potential core ends. The phase velocity varies with the axial distance; first decreasing and then increasing in velocity. According to theory, when the instability wave has a phase velocity that is supersonic relative to the ambient flow then the wave radiates noise. This criterion is expressed by the equation

$$|\overline{u}_m - c_{ph}| > \frac{\overline{u}_m}{M_m}. \qquad (12)$$

Using the flow conditions for the outer shear layer of Case 1 in equation (12), we find that when $c_{ph} > 0.393$, the phase velocity is supersonic relative to ambient conditions ($m = \infty$). Hence, all the phase velocities shown in Figure 5 for the different Strouhal number instability waves have both subsonic and supersonic regions.

The stability characteristics for the inner shear layer, shown in Figure 6, are quite different than the outer shear layer stability characteristics. For this case, all the different Strouhal number modes calculated continue to grow past the end of the outer potential core and do not begin to decay until the inner and the outer shear layers are almost fully merged together. While in the near nozzle potential core region, $c_{ph} > 1.102$ is required for the instability wave to be supersonic relative to the secondary flow ($m = 2$ in equation (12)), downstream of the outer potential core where the waves are attaining their

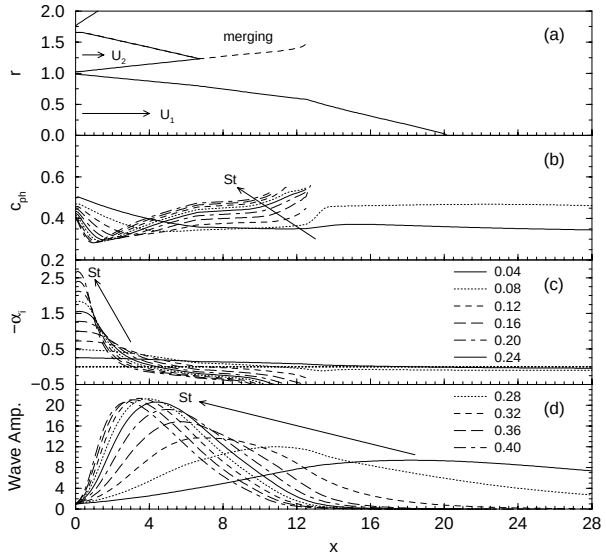

Figure 5: Stability characteristics for the $n = 1$ mode in the outer shear layer, Case 1. Calculated results for ten Strouhal numbers shown in the legend. (a) Edges of the shear layers in the velocity field; (b) phase velocity relative to U_1; (c) growth rate; (d) instability wave amplitude.

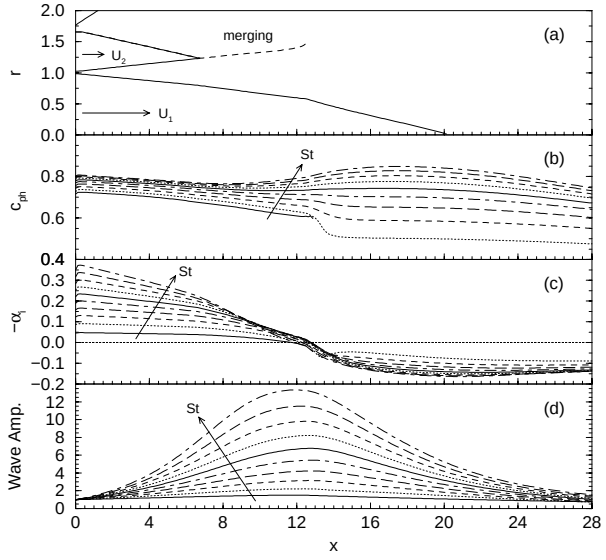

Figure 6: Stability characteristics for the $n = 1$ mode in the inner shear layer, Cast 1. Calculated results for ten Strouhal numbers. (a) Edges of the shear layers in the velocity field; (b) phase velocity relative to U_1; (c) growth rate; (d) instability wave amplitude. See Figure 5 for legend.

maximum amplitude, the condition for supersonic phase velocity is now relative to the ambient conditions. We see that the phase velocities are well above 0.393; the condition to create waves that radiate noise.

To show the components of the instability waves that radiate as noise, the wave number spectra calculated by equation (6) are shown in Figure 7(a) for both the inner and outer shear layer instability waves. As the Strouhal number increases, we see that the wave contains higher wave number content. The condition for far field noise radiation can be written in terms of the wave number coordinate η, defined in the Fourier transform of the instability wave in equation (6), as,[1]

$$\eta \leq \frac{\omega}{\overline{u}_\infty + c_\infty / U_1}. \tag{13}$$

On the figure, the location of the upper limit of equation (13) is shown labeled with the Strouhal number. At lower wave numbers (to the left of the indicator), the wave number components radiate noise and at higher wave numbers (to the right of the indicator), the wave number components do not radiate noise. We find that significant portions of the wave number components of the outer shear layer instability wave do not radiate noise to the far field. For the inner shear layer, the higher the Strouhal number, the more the wave number spectrum lies in the region where noise radiation can occur. Figure 7(a) represents the wave number spectrum of the noise source. Through the use of equation (5), the source is propagated to the far field. The resulting directivity patterns are shown in Figure 7(b). The upper limit of equation (13) translates to a directivity angle of zero degrees or along the jet exit axis.[1] As η decreases to zero, the directivity angle increases to 90 degrees. Therefore, since the peaks of the noise source spectra of the outer shear layer instability waves lie near this upper limit, that noise is directed downstream of the jet near the axis. In contrast, the inner shear layer noise sources radiate at larger angles to the jet exit axis.

The effect of changing the velocity ratio at constant mass flow, thrust and exit area on the stability characteristics is shown in Figure 8. In this example, the wave number spectra at $St = 0.12$ are shown for both the inner and the outer shear layer instability waves in each of the constant flow cases. As the velocity ratio decreases, the instability wave in the outer shear layer grows and decays more rapidly at a constant Strouhal number and with lower mean velocities in this shear layer, the phase velocity also decreases resulting in higher wave number components that do not radiate noise to the far field. In contrast, the inner shear layer gets larger and the wave number components of the instability wave that radiate noise grow larger in amplitude. To varying degrees, the dominance of the inner shear layer instability

waves in radiating noise to the far field occurs for all the Strouhal numbers calculated for the three constant flow condition cases.

Radiated Noise

We now consider the noise radiation characteristics of the instability waves in the coaxial jet compared to measured data. Since the initial amplitude of an instability wave at each frequency and mode is unknown, the calculated results shown here are qualitative and based on directivity characteristics.

The measured data shown in Figure 3 for Case 1 are replotted as function of the directivity angle at a fixed Strouhal number. Figure 9 compares calculated directivity curves to the measured data at different constant Strouhal numbers. The results for ten of those Strouhal numbers are shown in the figure. From the comparison in Figure 4, the large-scale structures were inferred to be the dominant noise sources radiating to at least a 60 degree angle from the jet exit axis. Furthermore, we showed in Figure 7 that only the inner shear layer instability waves, that continued to grow to their peak amplitude downstream of the outer potential core before decaying, radiated noise to large angles away from the jet exit axis. Thus, we show in Figure 9 the calculated directivity results, from using equation (5) for the $n = 1$ mode inner shear layer instability waves, for Case 1 with velocity ratio $U_2/U_1 = 0.58$. We see that the predicted peak directivity corresponds to the measured peak noise region, especially at higher Strouhal numbers. The subtle shifts in directivity that are predicted with increased Strouhal number are also followed by the measured data. As the Strouhal number increases, the peak directivity shifts to higher angles away from the axis.

Similar results for directivity comparisons are also found when we change the velocity ratio. Figure 10 shows calculated results compared to measured data at four Strouhal numbers for the three constant flow cases where U_2/U_1 decreases from 0.58 to 0.22. Except at the lowest Strouhal number, the predicted directivity of the $n = 1$ mode corresponds with the measured directivity. Dahl and Morris[1] predicted, for a different set of operating conditions, that the effect of decreasing the velocity ratio on inner shear layer instability wave noise radiation is to increase

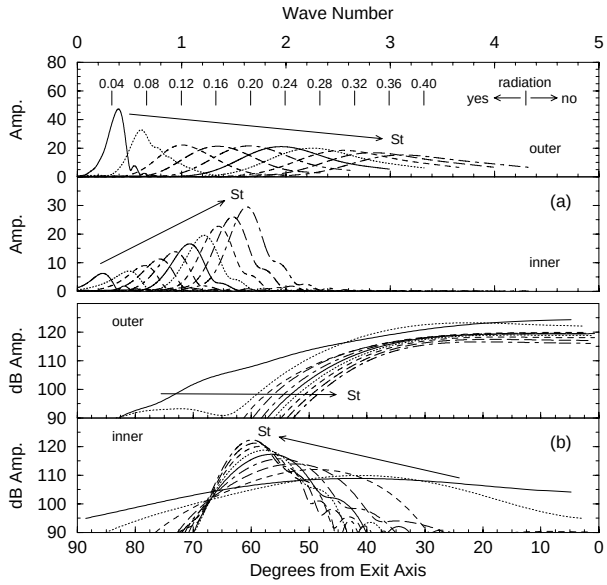

Figure 7: (a) Wave number spectra and (b) radiated noise directivity patterns for the $n = 1$ mode instability waves in the inner and outer shear layers, Case 1. Calculated results for ten Strouhal numbers. See Figure 5 for legend.

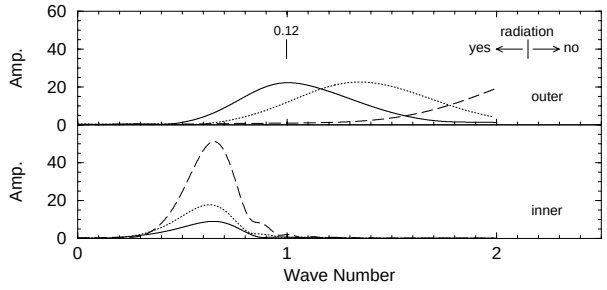

Figure 8: Wave number spectrum for the $n = 1$ mode instability wave, $St = 0.12$, in the inner and outer shear layers. Three constant flow conditions: (————) $U_2/U_1 = 0.58$; (· · · · · ·) $U_2/U_1 = 0.40$; (— — —) $U_2/U_1 = 0.22$.

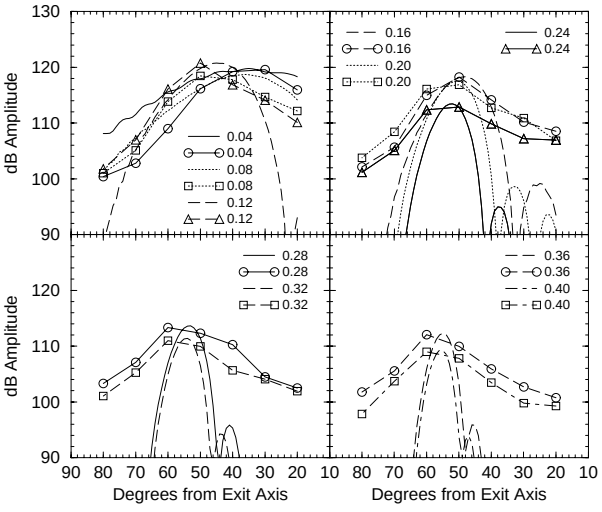

Figure 9: Comparison of measured directivities (symbols) at $r/D_1 = 80$ to calculated directivities (lines) for the $n = 1$ mode instability waves in the inner shear layer of Case 1 at ten Strouhal numbers.

the relative radiated noise level and to shift the peak of this noise radiation to lower angles at a given Strouhal number. The measured data for the three constant flow conditions shown in Figure 10 follow this trend.

Finally, the predicted directivity patterns shown in Figure 10 are much narrower than the measured directivity pattern at the higher Strouhal number. Tam and Chen[8] have shown calculated results for a Mach 2 single jet at a Strouhal number of 0.4 where there is significant contributions to the radiated noise from higher mode number instability waves; thus, broadening the peak. Figure 11 shows an example where the presence of multiple modes would have this effect. Here, the $n = 0$, 1, and 2 modes have been placed on the figure, without regard to their relative level, to show the possibility of broadening the predicted peak directivity pattern. Since at smaller angles the large-structure noise dominates, higher modes would be expected to be found. At large angles, fine-scale mixing is generating the noise.

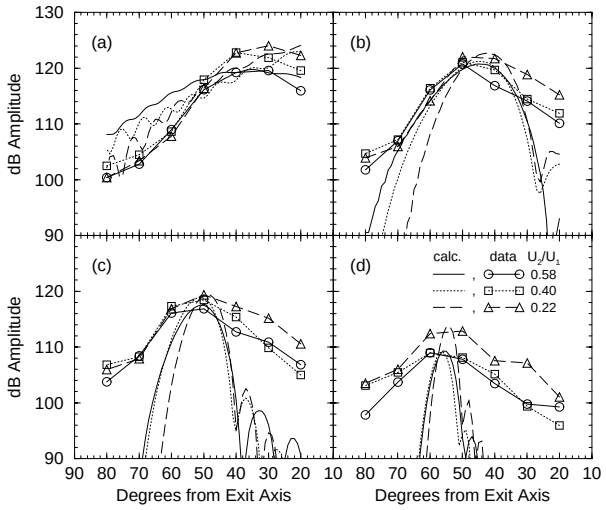

Figure 10: Comparison of measured directivities at $r/D_1 = 80$ to calculated directivities for the $n = 1$ mode instability waves in the inner shear layer of the three constant flow cases. (a) $St = 0.04$; (b) $St = 0.12$; (c) $St = 0.20$; (d) $St = 0.40$.

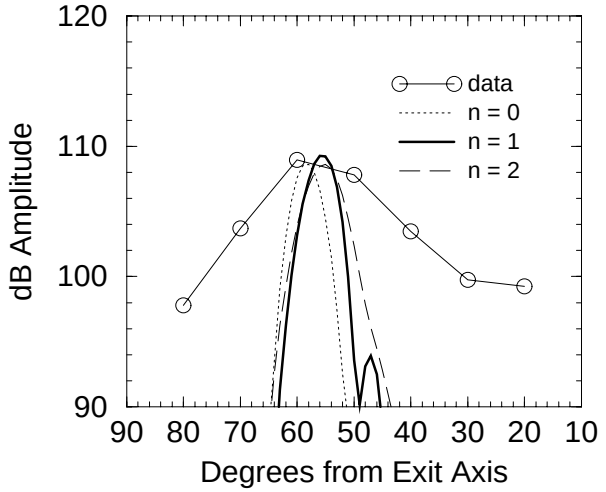

Figure 11: Comparison of measured directivity (circles) at $r/D_1 = 80$ to calculated directivities (lines) for three instability wave modes in the inner shear layer of Case 1 at $St = 0.40$.

Linearized Euler Calculations

The linearized Euler equation (LEE) solver was used to compute the disturbance field generated by the flow conditions given for Case 1. To avoid numerical difficulties due to the relatively thin initial shear layer, the shear layer was thickened from 1% to 10% of the jet radius. The computational grid extended axially over $0 \le x \le 70$ and radially over $0 \le r \le 32$, using 382 axial points and 276 radial points. In the axial direction, the grid was clustered near the nozzle exit plane with a spacing of $\Delta x = 0.08$, stretching to a spacing of $\Delta x = 0.23$ at the downstream exit plane of the computational grid. In the radial direction, the grid was uniform over $0 \le r \le 2$, with a spacing of $\Delta r = 0.02$. The grid then stretches smoothly to a spacing of $\Delta r = 0.23$ at the outer edge. This gives a minimum of 17 points per wavelength in the far field at $St = 0.2$, which is well within the resolution range of the solver. A time step of CFL = 1.4 was used in all computations. A computational run required 1.8 CPU hours on a Cray C90 and 8.3 megawords of memory. Using the Case 1 flow conditions, calculations were performed for the $n = 1$ mode with $St = 0.12$ and 0.20. The boundary conditions are discussed in Ref. [2].

Unlike the linear stability wave analysis, the disturbances in one shear layer can and will affect the disturbances in the other shear layer. Thus, it is hard to determine the contributions of each disturbance in the noise radiation pattern. In both of the cases tested ($St = 0.12$ and 0.20), two different inflow disturbances were specified in an attempt to distinguish the inner shear layer instability radiation from that of the outer shear layer.

The first disturbance, A_1, was centered on the inner shear layer and extended through the outer shear layer:

$$\begin{aligned} A_1(r,x) &= 0.5(1+\cos(\pi r_1)) \ , \ (r_1 \le 1) \\ &= 0 \qquad\qquad\qquad\quad , \ (r_1 > 1), \end{aligned} \tag{14}$$

where

$$r_1(r,x) = \sqrt{r^2 + x^2}$$

The second disturbance, A_2, was completely inside

the primary jet in an attempt to avoid exciting the outer shear layer:

$$\begin{aligned} A_2(r,x) &= 0.5(1+\cos(\pi r_2)) \ , \ (r_2 \le 1) \\ &= 0 \qquad\qquad\qquad\quad , \ (r_2 > 1), \end{aligned} \tag{15}$$

where

$$r_2(r,x) = \sqrt{(2r-1)^2 + (2x)^2}$$

Notice that neither A_1 or A_2 is an instability mode of the jet; thus, the amplitude and phase of the actual instability wave is unknown.

Figure 12 compares the amplitude of the pressure disturbance in the shear layers computed by the LEE solver to the instability wave amplitude computed for each shear layer using the linear stability analysis based on equation (2). The LEE pressure disturbance amplitude was obtained at the point in the shear layer where the axial velocity gradient in the radial direction is a maximum. When there are two distinct shear layers, there are two amplitudes. After the shear layers merge, there is one pressure disturbance amplitude. Figure 12(a) shows the LEE result for $St = 0.12$ using the A_1 input disturbance profile that excites both shear layers. Initially, A_1 excites the inner shear layer more than the outer shear layer. However, the outer shear layer disturbance grows to a larger amplitude than the inner shear layer disturbance until it merges with the inner shear layer disturbance near its peak amplitude. This peak coincides with the peak of the inner shear layer instability wave that was obtained from the stability analysis. If we try to excite only the inner shear layer instability using A_2, we get the result shown in Figure 12(b), where the pressure disturbance amplitude is greater in the inner shear layer compared to the amplitude in the outer shear layer. However, the growth and decay of the inner shear layer disturbance shows the same pattern as in Part (a); peaking at the same axial location.

There is less effect of the different initial disturbances on the solution $St = 0.20$, as shown in Figure 12(c) and 12(d). In both cases, the outer shear layer disturbance amplifies faster than the inner shear layer disturbance and begins to decay before merging with the inner shear layer disturbance. This agrees with the behavior obtained from the stability analysis for the two shear layers. The outer shear layer instability wave grows more rapidly than the inner shear layer instability wave and then decays rapidly as the inner shear layer instability wave continues to grow. When the shear layers merge, the inner shear layer instability wave reaches its maximum amplitude. Downstream, the amplitude of the LEE pressure disturbance decays slowly in the axial direction in a manner similar to the inner shear layer instability wave.

Figure 13 compares calculated directivity patterns to measured data along a line where $r/D_1 = 16$. For $St = 0.12$, the directivity for the LEE results using A_1 resembles the outer shear layer directivity from the instability wave model. This indicates that the radiating pressure disturbance calculated by the LEE solver is controlled by the outer shear layer pressure disturbances set up by the A_1 initial condition. When we try to remove the outer shear layer initial excitation in the LEE calculation by using the A_2 initial condition, the main directivity peak, shown in Figure 13(a), shifts to higher angles for a

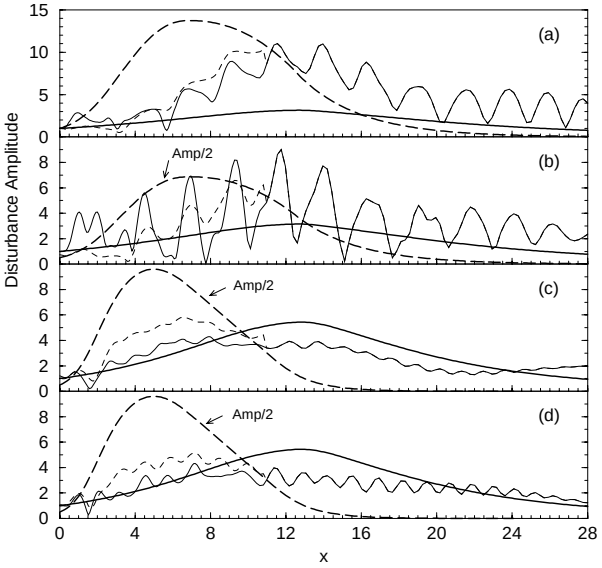

Figure 12: Comparison of pressure disturbance amplitudes for the $n = 1$ mode. (————) inner shear layer, LEE; (– – – –) outer shear layer, LEE; (▬▬▬) inner shear layer instability wave; (▬ ▬ ▬) outer shear layer instability wave. (a) $St = 0.12$, LEE using A_1; (b) $St = 0.12$, LEE using A_2; (c) $St = 0.20$, LEE using A_1; (d) $St = 0.20$, LEE using A_2.

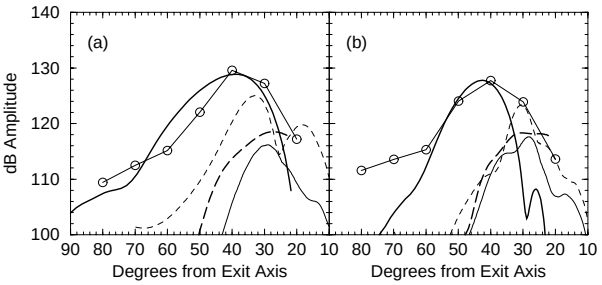

Figure 13: Comparison of measured directivity (circles) at $r/D_1 = 16$ to calculated directivities, $n = 1$ mode. (————) LEE using A_1; (– – – –) LEE using A_2; (▬▬▬) inner shear layer instability wave; (▬ ▬ ▬) outer shear layer instability wave. (a) $St = 0.12$; (b) $St = 0.20$.

closer agreement with the measured directivity data and the directivity pattern from the inner shear layer instability wave. This illustrates the effect of the inflow disturbance on the LEE radiation predictions. The initial amplitude and spatial variation of the disturbances are unknown and values chosen for them can affect the predicted noise radiation pattern.

Figure 13(b) shows the same set of comparisons for $St = 0.20$ that is shown in Part (a) for $St = 0.12$. If we consider the pressure disturbance results shown in Figure 12 for $St = 0.20$, we see that using the A_1 and A_2 initial conditions resulted in about the same pressure disturbance levels within both shear layers. As a result, the directivity patterns calculated by the LEE solver are peaking at about the same location, with some minor differences in the directivity patterns. But, in general, both the A_1 and A_2 initial conditions give peak directivities that resemble the outer shear layer instability wave directivity and do not compare well with both the measured data and the inner shear layer instability wave result. In this case, the LEE solver fails to produce the inner shear layer pressure disturbance characteristics that are required to produce the noise radiation directivity seen in the data.

CONCLUDING REMARKS

The measured noise spectrum generated by supersonic coaxial jets can be characterized by the same similarity spectra that Tam et al.[17] used to characterize single stream supersonic jets. With both sonic and subsonic secondary streams, large-scale structures generate the noise that dominates in the downstream direction from the jet. Using instability wave analysis, we showed that this noise, for the cases studied, was generated by instability waves originating in the inner shear layer and reaching their maximum amplitude downstream of the outer potential core where the two shear layers merge.

Using coaxial jet operating conditions where the total thrust, mass flow, and exit area were held constant, the measured noise followed trends predicted by instability wave noise theory. As the velocity ratio decreased, the radiated noise increased and the peak noise direction shifted to lower angles to the jet axis.

Finally, calculations were performed using a linearized Euler equation solver. Though the computed pressure disturbances within the jet had similar behavior to instability wave theory results, the radiated noise predicted did not compare well to the measured data. Further work is being performed using the LEE method to gauge the effects of the input disturbance, and to study the coupling of the instability waves between the two shear layers.

REFERENCES

1. M. D. Dahl and P. J. Morris. Noise from supersonic coaxial jets, part 2: Normal velocity profile. *J. Sound Vib.*, 200:665–699, 1997.
2. R. Hixon, S. H. Shih, and R. R. Mankbadi. Effects of coannular flow on linearized Euler equation predictions of jet noise. Paper No. 97-0284, AIAA, 1997.
3. D. Papamoschou. Mach wave elimination in supersonic jets. *AIAA J.*, 35:1604–1611, 1997.
4. D. Papamoschou and M. Debiasi. Noise measurements in supersonic jets treated with the Mach wave elimination method. Paper No. 98-0280, AIAA, 1998.
5. C. K. W. Tam and D. E. Burton. Sound generated by instability waves of supersonic flows. part 2. Axisymmetric jets. *J. Fluid Mech.*, 138:273–295, 1984.
6. C. K. W. Tam, P. Chen, and J. M. Seiner. Relationship between instability waves and noise of high-speed jets. *AIAA J.*, 30:1747–1752, 1992.
7. J. M. Seiner, T. R. S. Bhat, and M. K. Ponton. Mach wave emission from a high temperature supersonic jet. Paper No. 93-0734, AIAA, 1993.
8. C. K. W. Tam and P. Chen. Turbulent mixing noise from supersonic jets. Paper No. 93-4408, AIAA, 1993.
9. M. D. Dahl and P. J. Morris. Noise from supersonic coaxial jets, part 1: Mean flow predictions. *J. Sound Vib.*, 200:643–663, 1997.
10. C. K. W. Tam and F. Q. Hu. On the three families of instability waves of high-speed jets. *J. Fluid Mech.*, 201:447–483, 1989.
11. R. Hixon. On increasing the accuracy of MacCormack-type schemes for aeroacoustic applications. Paper No. 97-1586, AIAA, 1997.
12. H. K. Tanna. Coannular jets – are they really quiet and why? *J. Sound Vib.*, 72:97–118, 1980.
13. H. K. Tanna and P. J. Morris. The noise from normal-velocity-profile coannular jets. *J. Sound Vib.*, 98:213–234, 1985.
14. M. R. Bassiouni and D. S. Dosanjh. Acoustic and flow characteristics of cold high-speed coaxial jets. *AIAA J.*, 17:153–159, 1979.
15. J. M. Seiner, M. K. Ponton, B. J. Jansen, and N. T. Lagen. The effects of temperature on supersonic jet noise emission. Paper No. 92-02-046, DGLR/AIAA, 1992.
16. J. R. Stone, D. E. Groesbeck, and C. L. Zola. Conventional profile coaxial jet noise prediction. *AIAA J.*, 21:336–342, 1983.
17. C. K. W. Tam, M. Golebiowski, and J. M. Seiner. On the two components of turbulent mixing noise from supersonic jets. Paper No. 96-1716, AIAA, 1996.

REPORT DOCUMENTATION PAGE

Form Approved
OMB No. 0704-0188

1. AGENCY USE ONLY (*Leave blank*)	2. REPORT DATE	3. REPORT TYPE AND DATES COVERED
	May 1998	Technical Memorandum

4. TITLE AND SUBTITLE

Supersonic Coaxial Jets: Noise Predictions and Measurements

5. FUNDING NUMBERS

WU–537–05–21–00

6. AUTHOR(S)

Milo D. Dahl, Dimitri Papamoschou, Ray Hixon

7. PERFORMING ORGANIZATION NAME(S) AND ADDRESS(ES)

National Aeronautics and Space Administration
Lewis Research Center
Cleveland, Ohio 44135–3191

8. PERFORMING ORGANIZATION REPORT NUMBER

E–11179

9. SPONSORING/MONITORING AGENCY NAME(S) AND ADDRESS(ES)

National Aeronautics and Space Administration
Washington, DC 20546–0001

10. SPONSORING/MONITORING AGENCY REPORT NUMBER

NASA TM—1998-207422
AIAA–98–2294

11. SUPPLEMENTARY NOTES

Prepared for the Fourth Aeroacoustics Conference cosponsored by the American Institute of Aeronautics and Astronautics and the Confederation of European Aerospace Societies, Toulouse, France, June 2–4, 1998. Milo D. Dahl, NASA Lewis Research Center, Dimitri Papamoschou, University of California, Irvine, California 92697, and Ray Hixon, NASA Lewis Research Center. Responsible person, Milo D. Dahl, organization code 5940, (216) 433–3578.

12a. DISTRIBUTION/AVAILABILITY STATEMENT

Unclassified - Unlimited
Subject Category: 71 Distribution: Nonstandard

This publication is available from the NASA Center for AeroSpace Information, (301) 621–0390.

12b. DISTRIBUTION CODE

13. ABSTRACT ***(Maximum 200 words)***

The noise from perfectly expanded coaxial jets was measured in an anechoic chamber for different operating conditions with the same total thrust, mass flow, and exit area. The shape of the measured noise spectrum at different angles to the jet axis was found to agree with spectral shapes for single, axisymmetric jets. Based on these spectra, the sound was characterized as being generated by large-scale turbulent structures or fine-scale turbulence. Modeling the large scale structures as instability waves, a stability analysis was conducted for the coaxial jets to identify the growing and decaying instability waves in each shear layer and predict their noise radiation pattern outside the jet. When compared to measured directivity, the analysis identified the region downstream of the outer potential core, where the two shear layers were merging, as the source of the peak radiated noise where instability waves, with their origin in the inner shear layer, reach their maximum amplitude. Numerical computations were also performed using a linearized Euler equation solver. Those results were compared to both the results from the instability wave analysis and to measured data.

14. SUBJECT TERMS

Supersonic coaxial jets; Noise radiation; Noise prediction; Noise reduction; Jet noise; Measurements

15. NUMBER OF PAGES

17

16. PRICE CODE

A03

17. SECURITY CLASSIFICATION OF REPORT	18. SECURITY CLASSIFICATION OF THIS PAGE	19. SECURITY CLASSIFICATION OF ABSTRACT	20. LIMITATION OF ABSTRACT
Unclassified	Unclassified	Unclassified	